

Full Control of non-symmetric molecules orientation using weak and moderate electric fields

Rosario González-Férez¹ and Juan J. Omiste^{2, a)}

¹⁾*Instituto Carlos I de Física Teórica y Computacional, and Departamento de Física Atómica, Molecular y Nuclear, Universidad de Granada, 18071 Granada, Spain*

²⁾*Departamento de Química Física, Universidad Complutense de Madrid, 28040 Madrid, Spain*

(Dated: 21 November 2023)

We investigate the full control over the orientation of a non-symmetric molecule by using moderate and weak electric fields. Quantum Optimal Control techniques allow us to orient any axis of 6-chloropyridazine-3-carbonitrile, which is taken as prototype example here, along the electric field direction. We perform a detailed analysis by exploring the impact on the molecular orientation of the time scale and strength of the control field. The underlying physical phenomena allowing for the control of the orientation are interpreted in terms of the frequencies contributing to the field-dressed dynamics and to the driving field by a spectral analysis.

I. INTRODUCTION

The interaction of external fields with molecules creates coherent superpositions of field-free rotational states^{1,2} with plethora of applications in a wide range of areas from stereodynamics³⁻⁵, high precision measurements⁶, to quantum information processing^{7,8}. This interaction allows for the creation and control of highly rotating molecular states, namely superrotors⁹⁻¹¹, the separation and manipulation of chiral molecules¹²⁻¹⁵, the orientation of proteins^{16,17}, the isotopic separation¹⁸, the controlled manipulation enantiomers of chiral molecules¹⁹,

The orientation of the molecule requires the angular confinement of a molecule-fixed axis along a laboratory-fixed one and a preferred direction of the electric dipole moment²⁰⁻²². For asymmetric molecules, the 3D orientation implies that the all three molecular axes of inertia are confined to laboratory fixed ones and a well defined direction of electric dipole moment^{23,24}. Certain complex molecular systems, such as, the planar molecule 6-chloropyridazine-3-carbonitrile and the chiral one bromochlorofluoromethane (CHBrClF), possess a permanent dipole moment which do not coincide with any inertia axis. For these systems, it may be necessary to control the orientation of a specific molecular axis different from the one defined by the electric dipole moment. Therefore, it is mandatory to design an specific protocol beyond brute force orientation²⁵ or standard mixed-field orientation^{20,22} to accurately restrict the position of a given axis, i. e., a given atom. Such a task could benefit from long-established algorithms, as the Quantum Optimal Control (QOC)²⁶, to accurately drive the molecular dynamics. The fundamental concept of QOC involves designing a driving field that optimizes a certain expectation value or a state population in a quantum system. This is done by solving a self-consistent set of equations,

for which several algorithms have been developed^{27,28}. QOC constitutes a powerful tool for manipulating the dynamics of quantum systems^{26,28,29}, including the control of qubits³⁰, population of vibrational states³¹, coupled spin dynamics³², among others. Regarding molecular orientation control, Krotov algorithm^{27,33,34} is used to design terahertz laser pulses³⁵, or to manipulate the permanent dipole orientation of molecular ensembles, as reported in various studies³⁶⁻³⁹. In addition, this algorithm has been used to optimize alignment of molecules immerse in a thermal bath^{40,41}.

In this work, we consider a non-symmetric molecule, and apply the QOC algorithm to optimize the orientation of any molecular axis. Our study provides physical insights into the design of driving fields for this purpose. In particular, we provide a deeper understanding of the mechanisms underlying the control by means of a spectral analysis of the field-dressed wavepacket and of the driving field. This paper is organized as follows. [Section II](#) provides the Hamiltonian in an electric field, and a brief overview of the QOC theory with the corresponding equations of motion. In [Section III](#), we present the QOC results for the planar molecule 6-chloropyridazine-3-carbonitrile (CPC), taken here as a prototype example, orienting its permanent dipole moment and principal axes of inertia within the molecular plane, while varying the control field strength and duration. Finally, [Section IV](#) summarizes the main findings of the study and presents a short outlook.

II. THEORY AND METHODS

A. The Hamiltonian

In this work we investigate the orientation of a planar molecule without rotational symmetry by means of an external time-dependent electric field $\vec{E}(t)$, which is taken parallel to the Laboratory Fixed Frame (LFF) Z -axis. We work within the Born-Oppenheimer and the rigid rotor approximation, therefore, the molecular sys-

^{a)}Electronic mail: jomiste@ucm.es

tem is described by the Hamiltonian

$$H(t) = H_{rot} + H_E(t), \quad (1)$$

where $H_{rot} = B_x J_x^2 + B_y J_y^2 + B_z J_z^2$ is the field-free Hamiltonian, J_k the projection of the angular momentum operator \vec{J} along the k axis of the molecular fixed frame (MFF). The field-free rotational states are denoted by $J_{K_a, K_c} M^{42}$, where J is the total angular momentum number and M the magnetic quantum number, i. e., the projection of \vec{J} along the LFF Z -axis, and K_a and K_c are the projection of \vec{J} along the MFF z -axis in the prolate and oblate limiting cases, respectively.

The coupling of the molecular electric dipole moment $\vec{\mu}$ with an electric field parallel to the LFF Z -axis^{25,43} reads

$$\begin{aligned} H_E(t) &= -\vec{\mu} \cdot \vec{E}(t) = -E(t)\mu \cos \theta_{Z\mu} = \\ &= -E(t) (\mu_z \cos \theta_{Zz} + \mu_x \cos \theta_{Zx}) \end{aligned} \quad (2)$$

with being $\theta_{Z\mu}$ the angle between $\vec{\mu}$ and the LFF Z -axis, and θ_{Zk} the Euler angle between the molecular k axis and LFF Z -axis⁴⁴. The effect of this interaction is to orient the electric dipole moment along the electric field direction, which we characterize by $\langle \cos \theta_{Z\mu} \rangle$, with $\theta_{Z\mu}$ being the angle formed by the permanent dipole moment with the LFF Z -axis. In this work, we also explore the orientation of the MFF z and x axes along this LFF Z -axis in terms of $\langle \cos \theta_{Zz} \rangle$ and $\langle \cos \theta_{Zx} \rangle$, respectively.

B. Quantum Optimal Control

The goal of this work is to optimize the orientation of any molecular axis of an asymmetric planar molecule by using the Quantum Optimal Control (QOC) methodology to design a time-dependent electric field while imposing certain restrictions. To do so, we define the following functional²⁷

$$\mathcal{J}(\chi, \psi, E, \alpha) = \mathcal{J}_S(\chi, E, \psi) + \mathcal{J}_p(E, \alpha) + \mathcal{J}_o(\psi) \quad (3)$$

and seek for stationary trajectories in the system variables, i. e., the driving field $E(t)$ and the wavefunction $\psi(t)$ ⁴⁵. The first term in $\mathcal{J}(\chi, \psi, E, \alpha)$, guarantees that the time-dependent Schrödinger equation is fulfilled by introducing the Lagrange multiplier $\chi(t)$

$$\mathcal{J}_S(\chi, E, \psi) = -2 \text{Im} \left[\int_{T_0}^T dt \langle \chi(t) | i\partial_t - H(t) | \psi(t) \rangle \right], \quad (4)$$

where Im denotes the imaginary part, and T_0 and T are the initial propagation time and the measuring time, respectively. The penalty functional $\mathcal{J}_p(E, \alpha)$ reads as

$$\mathcal{J}_p(E, \alpha) = -\alpha \int_{T_0}^T dt \frac{E(t)^2}{S(t)}, \quad (5)$$

and forces a low fluence of the field by tuning the mask function $S(t)$ and a penalty factor α . The last term $\mathcal{J}_o(\psi)$ maximizes the expectation value of the operator O at the final time $t = T$

$$\mathcal{J}_o(\psi) = \langle \psi(T) | O | \psi(T) \rangle. \quad (6)$$

Note that the stationary trajectory fulfils that $\mathcal{J}_S(\chi, E, \psi) = 0$ and maximizes (minimizes) $\mathcal{J}_p(E, \alpha) + \mathcal{J}_o(\psi)$. To achieve the latter, the values of α and the function $S(t)$ must be carefully chosen such that the contribution of the fluence of $E(t)$ is small compared to $\langle O \rangle$.

The QOC equations²⁷ are obtained by solving the Euler equation associated to the functional $\mathcal{J}(\chi, \psi, E, \alpha)$ Eq. (3), and are given by

$$i\partial_t \psi(t) - H(t)\psi(t) = 0, \quad (7)$$

$$i\partial_t \chi(t) - H(t)\chi(t) = 0, \quad (8)$$

$$\chi(T) = O\psi(T), \quad (9)$$

$$\vec{E}(t) = -\frac{S(t)}{\alpha} \text{Im} [\langle \chi(t) | \vec{\mu} | \psi(t) \rangle], \quad (10)$$

and their complex conjugates. This self-consistent system of equations is solved using the Krotov method^{27,33,34}, which converges to a stationary solution for positive defined observable operators⁴⁶. Hence, to maximize the orientation $\langle \cos \theta_{Zk} \rangle$ and to ensure the convergence of the algorithm, we set $O = \cos \theta_{Zk} + 1$.

In order to describe the dynamics, we solve the time dependent Schrödinger equation associated to the Hamiltonian in Eq. (1). A basis set expansion of the wavefunction $\Psi(\Omega, t)$ is done in terms of the Wigner matrix elements⁴⁴, their most relevant properties and the matrix elements required are given in detailed elsewhere⁴⁴. In this basis expansion, we take into account that magnetic quantum number M is conserved, because the electric field $\vec{E}(t)$ is parallel to the LFF Z -axis. For the time propagation, we apply the short iterative Lanczos scheme⁴⁷.

III. RESULTS

As an example of non-symmetric planar molecules, we use 6-chloropyridazine-3-carbonitrile (CPC), with rotational constants $B_x = 717.42$ MHz, $B_y = 639.71$ MHz and $B_z = 5905$ MHz⁴⁸. This molecule is characterized by having its electric dipole moment not parallel to any principal axis of inertia, as shown in [Figure 1](#), with $\mu = 5.20$ D and components $\mu_x = 4.37$ D and $\mu_z = 2.83$ D⁴⁸. We focus on the field-dressed dynamics of the rotational ground state. To provide a deeper physical insight into the QOC mechanism, we explore the orientation along the driving field direction of any molecular axis, i. e., the permanent dipole moment, $\vec{\mu}$, and the principal axes of inertia in the molecular plane x and z .

For the mask function of the electric field, we use a Gaussian envelope $S(t) = \exp\left(-\frac{4t^2 \ln 2}{\tau^2}\right)$, with τ being the Full Width at Half Maximum (FWHM). The

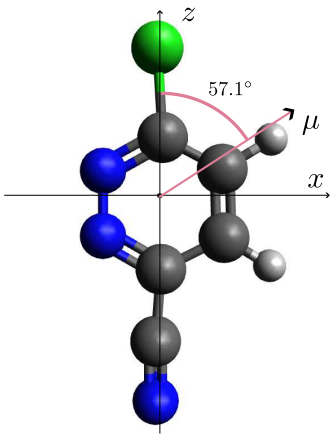


FIG. 1. Sketch of the molecular structure of 6-chloropyridazine-3-carbonitrile (CPC). The molecular geometry and the dipole moment, $\vec{\mu}$, are taken from Ref. 48.

time interval is set to $[T_0, T] = [-2.53\tau, 2.53\tau]$, taking $T = -T_0 = \sqrt{\frac{\ln 5 \cdot 10^7 \tau}{\ln 2} \frac{\tau}{2}}$ for computational convenience. The field-dressed dynamics is analyzed in terms of transition between field-free rotational states involved in the optimal control process. The most relevant transitions and their frequencies are collected in Table I. These frequencies also allow us to interpret the structure of the driving field in the forthcoming sections.

Transition	Frequency (GHz)	Transition	Frequency (GHz)
$0_{00}0 \leftrightarrow 1_{01}0$	1.35	$4_{04}0 \leftrightarrow 5_{05}0$	6.76
$1_{10}0 \leftrightarrow 2_{02}0$	2.47	$1_{01}0 \leftrightarrow 2_{11}0$	7.81
$1_{10}0 \leftrightarrow 2_{11}0$	2.63	$2_{02}0 \leftrightarrow 3_{12}0$	9.05
$1_{01}0 \leftrightarrow 2_{02}0$	2.71	$2_{20}0 \leftrightarrow 3_{12}0$	11.87
$2_{02}0 \leftrightarrow 3_{03}0$	4.06	$8_{08}0 \leftrightarrow 9_{18}0$	15.84
$3_{03}0 \leftrightarrow 4_{04}0$	5.41	$1_{10}0 \leftrightarrow 2_{20}0$	18.40
$0_{00}0 \leftrightarrow 1_{10}0$	6.53	$2_{20}0 \leftrightarrow 3_{30}0$	30.27

Table I. Transition frequencies between the main rotational states involved in the field-dressed dynamics.

A. Quantum Optimal Control for fixed penalty parameter α

In this section, we set $\alpha = 10^6$ for the driving electric field, which is equivalent to fixing its maximum allowed strength given by μ/α , and consider two different FWHMs τ . For a 1 ns-FWHM field, the results obtained when the expectation value $\langle \cos \theta_{Zz} \rangle$ is optimized are presented in Figure 2 (a)-(d). The driving field designs a wavepacket populating rotational states and adjusting their relative phases. The time-evolution of the quantum interferences between these populated states provokes that $\langle \cos \theta_{Zz} \rangle$ reaches a maximum at the final T

as shown in Figure 2 (a). During the time-evolution, the orientation varies between $\langle \cos \theta_{Zz} \rangle = -0.48$ and $\langle \cos \theta_{Zz} \rangle = 0.824$, and its oscillation pattern indicates that only a few states are involved in the dynamics. A spectral analysis of $\langle \cos \theta_{Zz} \rangle$ encounters three main frequencies 1.38, 2.77 and 4.15 GHz, associated to the transitions $0_{00}0 \leftrightarrow 1_{01}0$, $1_{01}0 \leftrightarrow 2_{02}0$ and $2_{02}0 \leftrightarrow 3_{03}0$, respectively, see Table I. These rotational states are linked by the selection rules $\Delta J = \pm 1$ and $\Delta M = 0$, imposed by the operator $\cos \theta_{Zz}$ ^{44,49} in Equation 2. For this optimization, the driving electric field in Figure 2 (d) is mostly relevant before $t = 0$ finding two main peaks at $t = -0.56$ ns and $t = -0.35$ ns with intensity 0.87 kV/cm and -1 kV/cm, respectively, being very weak afterwards. This control field is also mainly formed by these transition frequencies, as illustrated by the square of its Fourier Transform $|\mathcal{F}[E(t)]|^2$ in Figure 3. Note that $|\mathcal{F}[E(t)]|^2$ is normalized so its maximum value is 1. The wide peaks of the $\tau = 1$ ns field are due to the duration imposed in the optimization algorithm. One can distinguish the frequencies 1.35, 4.06 and 5.41 GHz, associated to the transitions $0_{00}0 \leftrightarrow 1_{01}0$, $2_{02}0 \leftrightarrow 3_{03}0$ and $3_{03}0 \leftrightarrow 4_{04}0$, respectively. Note that the contribution of the latter in the orientation pattern is negligible. The frequency 2.77 GHz from the $1_{01}0 \leftrightarrow 2_{02}0$ transition is blurred due to the overlap with the preceding peaks. Despite the field being designed to optimize $\langle \cos \theta_{Zz} \rangle$, we encounter a moderate orientation of the molecular x -axis in Figure 2 (c) due to the coupling through μ_x . The orientation $\langle \cos \theta_{Zx} \rangle$ faithfully follows the external field until $t \approx 0.5$ ns. From there on the field is very small, and $\langle \cos \theta_{Zx} \rangle$ oscillates with a small amplitude reaching $\langle \cos \theta_{Zx} \rangle = -0.028$ at $t = T$. Reaching this almost zero orientation is possible since the time scale required for the x -axis dynamics is shorter than the period of oscillation of the electric field. Hence the impact of the driving field averages out due to the rapid oscillation of the molecule. The frequency of the x axis orientation is determined by the rotational constants of the orthogonal axes, namely B_y and B_z , which have an average value of approximately 3.27 GHz. This frequency is greater than the oscillation frequency of the driving field, which is around 1.6 GHz. The spectral analysis of $\langle \cos \theta_{Zx} \rangle$ confirms that the states $1_{10}0$, $2_{11}0$ and $3_{12}0$ are also populated in the field-dressed dynamics. For the sake of completeness, we present $\langle \cos \theta_{Z\mu} \rangle$ in Figure 2(c), which shows a similar behaviour as $\langle \cos \theta_{Zz} \rangle$.

The driving field and the dressed rotational dynamics are highly complex when the QOC technique is applied to the orientation of the molecular x -axis. In Figure 2 (f), $\langle \cos \theta_{Zx} \rangle$ shows a complex oscillatory behaviour, which is due to the different time scale associated with the dynamics along this axis. At $t = T$ a large orientation is reached $\langle \cos \theta_{Zx} \rangle \approx 0.83$. The driving field is presented in Figure 2 (h), $E(t)$ rapidly oscillates for $t \lesssim 0.5$ ns, which contrasts with the slow oscillations of field optimizing $\langle \cos \theta_{Zz} \rangle$ in Figure 2 (d). This behaviour agrees with the rapid rotational dynamics of the MFF x -axis indicated above, and $\langle \cos \theta_{Zx} \rangle$ follows the field oscillations

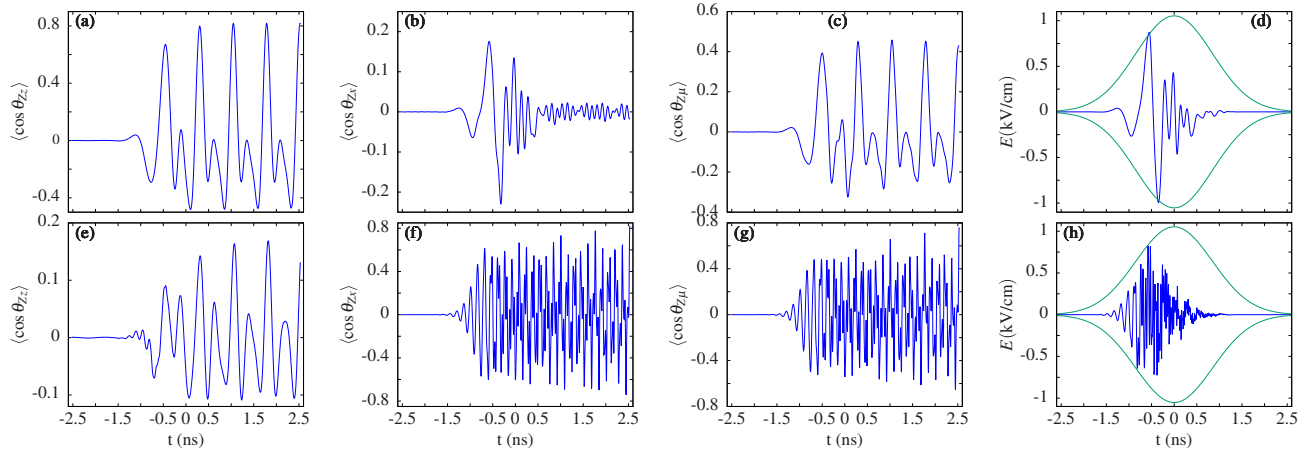


FIG. 2. Optimization of $\langle \cos \theta_{Zz} \rangle$ (panels (a)-(d) in the upper row) and $\langle \cos \theta_{Zx} \rangle$ (panels (e)-(h) in the lower row) for the initial state $|0_{00}0\rangle$. (a) and (e): $\langle \cos \theta_{Zz} \rangle$; (b) and (f): $\langle \cos \theta_{Zx} \rangle$; (c) and (g): $\langle \cos \theta_{Z\mu} \rangle$; and (d) and (h): optimal electric field $E(t)$ and mask function $\pm \frac{S(t)}{\alpha}$ as a function of time. The parameters τ and α are set to 1 ns and 10^6 , respectively.

in Figure 2 (f). The Fourier Transform of $\langle \cos \theta_{Zx} \rangle$ shows three main frequencies, namely, 6.45 GHz, 18.47 GHz and 30.40 GHz, associated to the transitions $|0_{00}0\rangle \leftrightarrow |1_{10}0\rangle$, $|1_{10}0\rangle \leftrightarrow |2_{20}0\rangle$ and $|2_{20}0\rangle \leftrightarrow |3_{30}0\rangle$, respectively. Now, the orientation of the dipole moment along the LFF Z -axis $\langle \cos \theta_{Z\mu} \rangle$, see Figure 2 (g) follows a similar behaviour as $\langle \cos \theta_{Zx} \rangle$, and a significant value is reached at $t = T$ with $\langle \cos \theta_{Z\mu} \rangle = 0.76$.

In contrast, $\langle \cos \theta_{Zz} \rangle$ is incapable of adjusting to the rapidly changing driving field as observed in Figure 2 (e). Indeed, the control field in Figure 2 (h) imprints short transfers of momentum at each cycle, similar to the impulsive alignment described for short laser pulses¹. As a consequence, the amplitude of $\langle \cos \theta_{Zz} \rangle$ cannot be efficiently reduced at the final time in general. To bypass this effect, the algorithm fine tunes all the relative quantum phases within the wavepacket, seeking for reducing the orientation of the z -axis, i. e., approaching it to zero, at the final time $t = T$. However, if the pulse duration is short compared to the time characteristic of the z -axis dynamics, the oscillation may not vanish. This is the case in Figure 2 (e), where the orientation of the

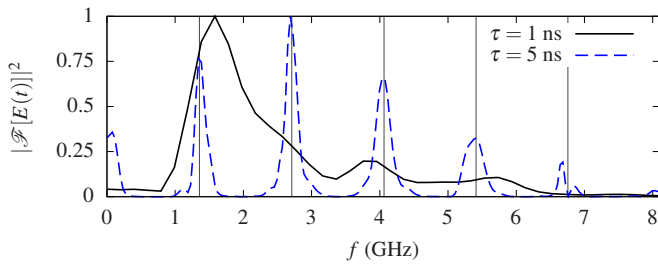


FIG. 3. For $\alpha = 10^6$ and FWHMs $\tau = 1$ and 5 ns, the absolute squared Fourier Transform of the optimized electric field, $|\mathcal{F}[E(t)]|^2$ to maximize $\langle \cos \theta_{Zz} \rangle$. Note that $|\mathcal{F}[E(t)]|^2$ is normalized so that the absolute maximum equals 1.

molecular z -axis is not negligible, i. e., $\langle \cos \theta_{Zz} \rangle \approx 0.16$, at $t = T$, which is due to the short FWHM, $\tau = 1$ ns, of the driving field.

We now consider an optimizing field with $\tau = 5$ ns FWHM, and explore the results of the QOC algorithm applied to the three possible orientation axes. Compared to the 1 ns pulse in Figure 2 (a), $\langle \cos \theta_{Zz} \rangle$ exhibits faster oscillations with large amplitude, which increase till the maximal value $\langle \cos \theta_{Zz} \rangle = 0.9$ at $t = T$. The optimized electric field, see Figure 4 (a), also possesses rapid oscillations mainly for $t \lesssim 0$ ns when the rotational wavepacket is created. In particular, for $t \lesssim -3.5$ ns, $\langle \cos \theta_{Zz} \rangle$ follows this driving field. The spectral analysis given by the Fourier Transform of the field in Figure 3 presents clearly defined and well separated peaks. This larger FWHM allows to populate highly excited rotational states associated to the additional frequency 6.76 GHz of the $|4_{04}0\rangle \leftrightarrow |5_{05}0\rangle$ transition. Panels (b) and (c) of Figure 4 present the orientation of the MFF x axis and $\vec{\mu}$ along the LFF Z -axis. As in the previous case, the behaviour of $\langle \cos \theta_{Z\mu} \rangle$ resembles $\langle \cos \theta_{Zz} \rangle$, but reaching smaller final value with $\langle \cos \theta_{Z\mu} \rangle = 0.502$ at $t = T$. In contrast, $\langle \cos \theta_{Zx} \rangle$ shows rapid oscillations of small amplitude for $t > 0$ ns, and at $t = T$ $\langle \cos \theta_{Zx} \rangle = 0.015$.

The results obtained when $\langle \cos \theta_{Zx} \rangle$ is optimized are shown in Figure 4 (e)-(h). The driving field in Figure 4 (h), presents a more complex structure with faster and narrower oscillations compared to the previous field in Figure 4 (d). The number of rotational states contributing to the field-dressed dynamics is enhanced, as it is manifested in the irregular oscillations of $\langle \cos \theta_{Zz} \rangle$, $\langle \cos \theta_{Zx} \rangle$ and $\langle \cos \theta_{Z\mu} \rangle$ in Figure 4 (e), (f) and (g), respectively. During the time evolution, $\langle \cos \theta_{Zz} \rangle$ shows moderate values, but the field is adjusted to reduce it at $t = T$ attaining $\langle \cos \theta_{Zz} \rangle \approx 0.019$. In contrast, the orientation of the MFF x -axis is significantly enhanced to $\langle \cos \theta_{Zx} \rangle \approx 0.92$ at $t = T$, and $\langle \cos \theta_{Z\mu} \rangle$ presents a similar behaviour.

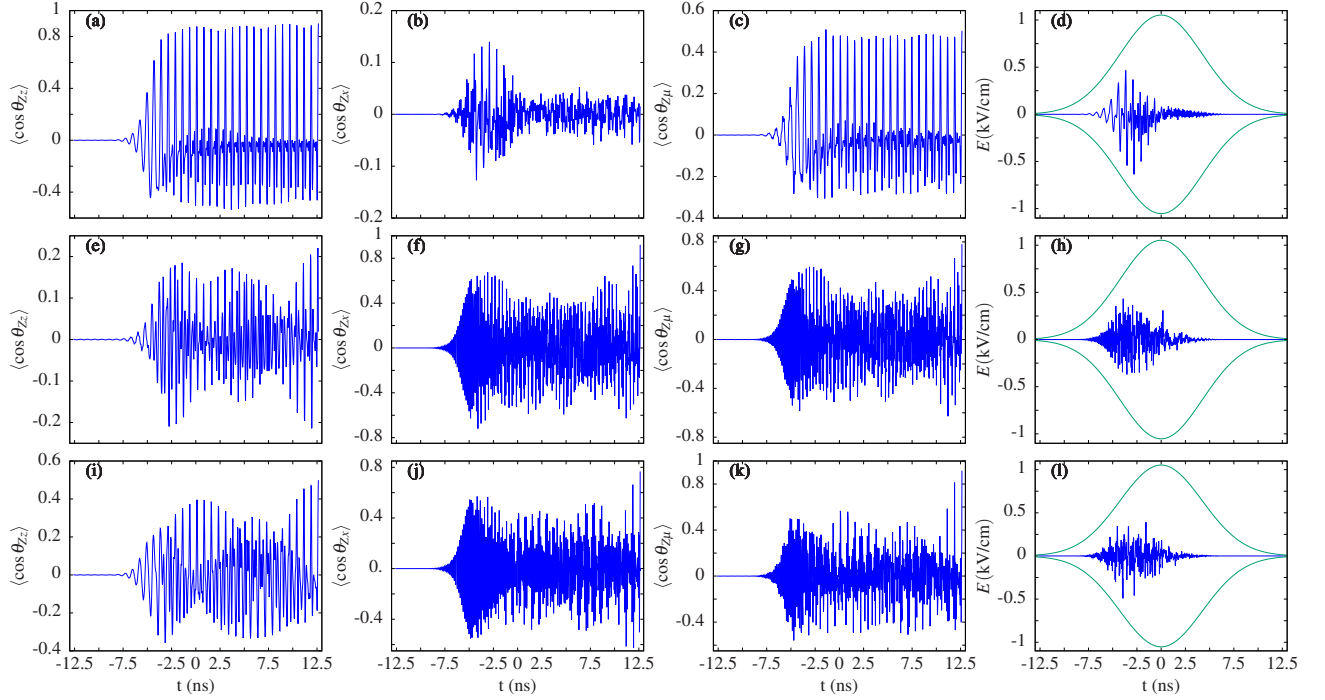


FIG. 4. Optimization of $\langle \cos \theta_{Zz} \rangle$ (panels (a)-(d) in the upper row) and $\langle \cos \theta_{Zx} \rangle$ (panels (e)-(h) in the middle row) and $\langle \cos \theta_{Z\mu} \rangle$ (panels (i)-(l) in the lower row) for the initial state $0_{00}0$. (a), (e) and (i): $\langle \cos \theta_{Zz} \rangle$; (b), (f) and (j): $\langle \cos \theta_{Zx} \rangle$; (c), (g) and (k): $\langle \cos \theta_{Z\mu} \rangle$; and (d), (h) and (l): optimal electric field $E(t)$ and mask function $\pm \frac{S(t)}{\alpha}$ as a function of time. The parameters τ and α are set to 5 ns and 10^6 , respectively.

For completeness, we present the optimization of the orientation of the dipole-moment axis in Figure 4 (i)-(l). In this case, the quantum interference is constructive for $\langle \cos \theta_{Zx} \rangle$ and $\langle \cos \theta_{Zz} \rangle$, having both a local maximum at $t = T$ ($\langle \cos \theta_{Zz} \rangle \approx 0.50$ and $\langle \cos \theta_{Zx} \rangle \approx 0.77$, whereas $\langle \cos \theta_{Z\mu} \rangle \approx 0.92$). This illustrates that the orientation of the permanent dipole moment is largely dominated by its x component. The spectral analysis of $E(t)$ shows that the transitions collected in Table I are relevant for the QOC, i.e., these rotational states build up the control dynamics and maximal orientation of $\vec{\mu}$.

B. Quantum Optimal Control for varying the penalty factor α

In this section, we investigate the QOC orientation for different values of α , i.e., the maximum allowed strength of the control field, which is represented by the factor μ/α . For $\tau = 1$ and 5 ns, we present in Figure 5 the final optimized orientation as a function of the penalty factor α . Our analysis reveals that for a given α and τ , optimizing $\langle \cos \theta_{Zx} \rangle$ results in a larger orientation compared to $\langle \cos \theta_{Zz} \rangle$. This finding supports the idea that QOC is more effective when the natural timescale of the degree of freedom being optimized is smaller than the field duration, as discussed in Section III A. Moreover, for a given α , the larger the FWHM the better the optimized orientation is, for both $\langle \cos \theta_{Zx} \rangle$ and $\langle \cos \theta_{Zz} \rangle$.

Our analysis also reveals that, for the values of α considered, $\langle \cos \theta_{Zx} \rangle$ decreases as a function of α , meaning that stronger fields result in larger optimized orientations. Note that for both FWHMs, $\langle \cos \theta_{Zx} \rangle$ is very similar for $\alpha = 10^5$ and 10^6 , i.e., the orientation saturates beyond certain intensities of the driving field. Since the orientation is not increasing, the functional $\mathcal{J}_o + \mathcal{J}_p$ is maximized by minimizing the fluence of the field, involved in the penalty functional, \mathcal{J}_p . This saturation of

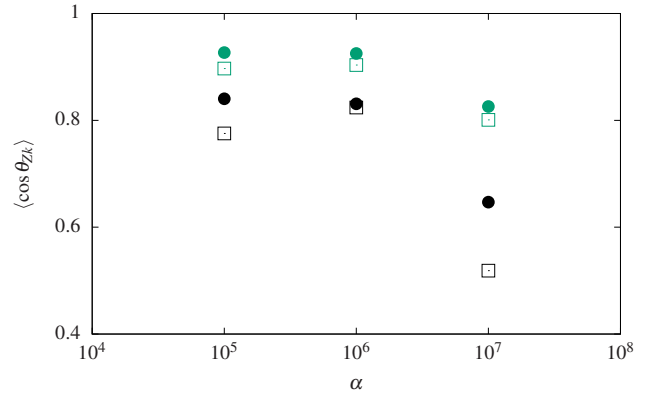


FIG. 5. Final orientations of the MFF x (bullets) and z (squares) axes, $\langle \cos \theta_{Zx} \rangle$ and $\langle \cos \theta_{Zz} \rangle$, respectively, after applying QOC using electric fields with FWHM $\tau = 1$ (black) and 5 ns (green) as a function of the penalty factor α .

$\langle \cos \theta_{Zx} \rangle$ with α can be explained in terms of the brute force orientation occurring at these strong fields, combined with the larger frequencies along the MFF x -axis facilitating that the molecule follows the driving field. Furthermore, for $\alpha = 10^5$, that is, the stronger field case, the population transfer may not be understood in terms of one-photon transition, but as a strong field process.

In contrast, the orientation of the MFF z -axis decreases as α decreases, i. e., as the maximal field strength increases. This is due to the strong dependence of the controllability of the orientation of this axis on the process for the suppression of $\langle \cos \theta_{Zx} \rangle$ imposed by the QOC equations. Note that the faster dynamics of the x axis and the larger component of $\vec{\mu}$ along x also play an important role against reducing $\langle \cos \theta_{Zx} \rangle$. Thus, achieving this suppression requires finely tuned quantum phases among the rotational states, as small changes can result in different outcomes. Besides, the QOC algorithm aims to maximize $\mathcal{J}_p(E, \alpha) + \mathcal{J}_o(\psi)$, as discussed in Section II B. However, due to the limited control of $\mathcal{J}_o(\psi)$, a better approach to the stationary point is reached for smaller $\mathcal{J}_o(\psi)$ and larger $\mathcal{J}_p(E, \alpha)$.

Finally, we perform an spectral analysis of the optimization along the x , z , and μ axes for the impact parameter $\alpha = 10^5$ and 10^7 and $\tau = 5$ ns. The Fourier transforms of the QOC fields are shown in Figure 6, together with the frequencies of the main transitions between field-free rotational states, which are also collected in Table I. In the weak field regime, $\alpha = 10^7$, shown in Figure 6 (a), we observe well-defined isolated frequencies for all the optimized orientation observables. The frequencies of $E(t)$ obtained from the optimization of $\langle \cos \theta_{Zz} \rangle$ and $\langle \cos \theta_{Zx} \rangle$ are different due to the different selection rules $\Delta K = 0$ and $\Delta K = \pm 1$ imposed by the operators μ_z and μ_x , respectively. For the initial state $0_{00}0$, the relevant transitions for the optimization of the z -axis orientation are $0_{00}0 \leftrightarrow 1_{01}0$, $1_{01}0 \leftrightarrow 2_{02}0$, and $2_{02}0 \leftrightarrow 3_{03}0$, which are characterized by frequencies of 1.35, 2.71, and 4.06 GHz, respectively. However, the optimization of $\langle \cos \theta_{Zx} \rangle$ is dominated by the frequencies mixing K , specifically $0_{00}0 \leftrightarrow 1_{10}0$ (6.53 GHz), $1_{10}0 \leftrightarrow 2_{02}0$ (2.47 GHz), $2_{02}0 \leftrightarrow 3_{12}0$ (9.05 GHz). The relatively low value of $\langle \cos \theta_{Zx} \rangle$ at $t = T$, see Figure 5, can be explained in terms of the relevant frequencies in $E(t)$ for the orientation of $\langle \cos \theta_{Zz} \rangle$ being below the frequency required to transfer population from $0_{00}0$ to $1_{10}0$, which is the first excited state coupled by μ_x . On the contrary, the transition frequencies of $0_{00}0 \leftrightarrow 1_{10}0$ and $2_{02}0 \leftrightarrow 3_{12}0$ are above the main transitions. This results in the impulsive orientation of the molecular Z -axis as discussed in Section III A. Additional frequencies are observed in Figure 6 (a) when the orientation of the permanent dipole moment is optimized, with two new peaks at 2.63 and 7.81 GHz due to $1_{10}0 \leftrightarrow 2_{11}0$ and $1_{01}0 \leftrightarrow 2_{11}0$, respectively.

For a strong control field with $\alpha = 10^5$, the spectrum becomes more complex due to two main reasons. Firstly, the contribution of more excited rotational states, such

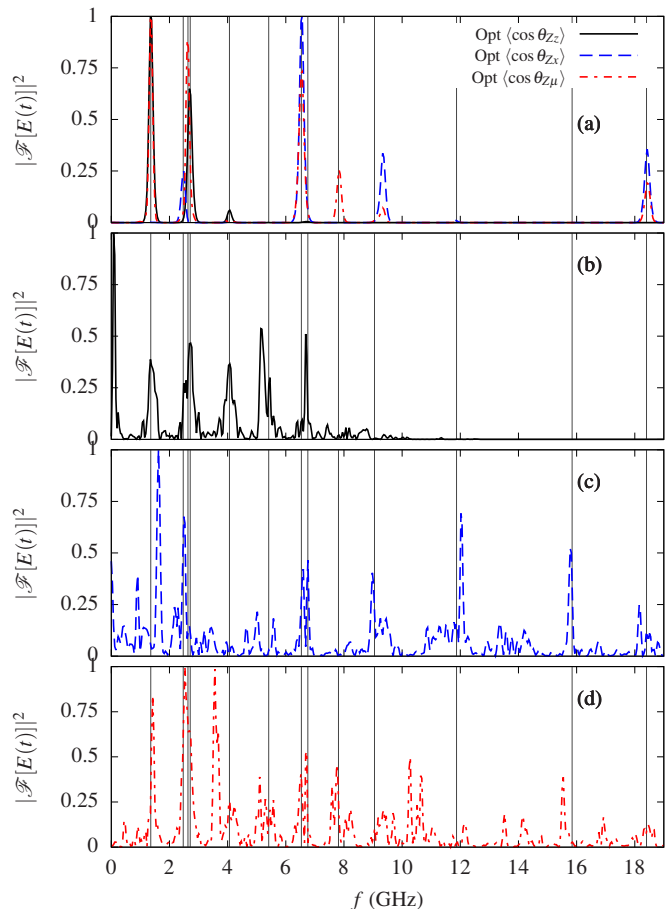


FIG. 6. For a pulse duration of $\tau = 5$ ns, the absolute squared Fourier Transform, $|\mathcal{F}[E(t)]|^2$, of the optimized electric field is shown for (a) $\alpha = 10^7$ and (b)-(d) $\alpha = 10^5$. The Fourier Transform plotted correspond to optimization of $\langle \cos \theta_{Zz} \rangle$ (solid black), $\langle \cos \theta_{Zx} \rangle$ (blue dashed) and taking as initial state $0_{00}0$. The vertical lines correspond to the transition frequencies shown in Table I. Note $|\mathcal{F}[E(t)]|^2$ is normalized so that the absolute maximum equals 1.

as the peak at 15.84 GHz corresponding to the transition $8_{08}0 \leftrightarrow 9_{18}0$, which appears for the orientation of the MFF x -axis along the LFF Z -axis. Secondly, the brute force orientation mediated by the large amplitude of the field, as reported in previous studies^{20,25}. Therefore, the driving field can not be simply described as the contribution of several frequencies, i. e., as population transfer mediated by absorption of several photons, due to the high intensity of the driving field, as we discussed in Section III B.

IV. CONCLUSIONS AND OUTLOOK

In this work, we have demonstrated the feasibility of fully controlling the orientation of any molecular axis of non-symmetric planar molecules by means of quantum

optimal control. The driving field is composed of just a few frequencies corresponding to transitions among several field-free states, and its temporal profile and strength can be reached experimentally. For a mask function with FWHM and weak strength, our findings show limited control due to the small population transfer stimulated due to the interaction with the field. On the contrary, the electric field cannot be described by isolated components for strengths above 1 kV/cm, since the number of transitions among the involved states increases and they overlap due to their spectral width. This effect is further enhanced for short pulses. This work shows the efficiency, flexibility and potential of QOC for the rotational dynamics control of non-symmetric molecules, and provides valuable insights into the conditions required for it.

This study focus on the stereodynamics of the ground state of CPC, and without loss of generality, the results could be extended to excited states. This technique provides an alternative strategy to the mixed-field orientation method, which, in the case of CPC, was shown to attain full control of only one molecular axis^{48,50}.

Summing up, we have demonstrated that QOC is a powerful technique to control the orientation of any planar molecule without rotational symmetry, and, furthermore, to more complex systems as enantiomers. Indeed, the manipulation, control and selection of chiral molecules^{14,51,52} will have a enormous impact on the pharmaceutical industry, where the spatial arrangement of the atoms in one enantiomer may determine the biological activity of a drug, as the remarkable case of thalidomide⁵³. Moreover, the design of optimally designed chiral electric fields could be used to efficiently create oriented superrotor states¹².

ACKNOWLEDGMENTS

J.J.O. acknowledges the funding by the Madrid Government (Comunidad de Madrid Spain) under the Multiannual Agreement with Universidad Complutense de Madrid in the line Research Incentive for Young PhDs, in the context of the V PRICIT (Regional Programme of Research and Technological Innovation) (Grant: PR27/21-010), spanish projects PID2019-105458RB-I00 and PID2021-122839NB-I00 (MICIN). R.G.F. gratefully acknowledges financial support by the Spanish projects PID2020-113390GB-I00 (MICIN), PY20_00082 (Junta de Andalucía), and A-FQM-52-UGR20 (ERDF-University of Granada) and the Andalusian research group FQM-207. We would also like to thank Ignacio Solá for fruitful discussions.

¹H. Stapelfeldt and T. Seideman, “Colloquium: Aligning molecules with strong laser pulses,” *Rev. Mod. Phys.* **75**, 543–557 (2003).

²C. P. Koch, M. Lemeshko, and D. Sugny, “Quantum control of molecular rotation,” *Rev. Mod. Phys.* **91**, 035005 (2019), arXiv:1810.11338.

- ³D. R. Herschbach, “Chemical stereodynamics: retrospect and prospect,” *Eur. Phys. J. D* **38**, 3–13 (2006).
- ⁴V. Aquilanti, M. Bartolomei, F. Pirani, D. Cappelletti, and F. Vecchiocattivi, “Orienting and aligning molecules for stereochemistry and photodynamics,” *Phys. Chem. Chem. Phys.* **7**, 291–300 (2005).
- ⁵D. Yang, D. Xie, and H. Guo, “Stereodynamical Control of Cold Collisions of Polyatomic Molecules with Atoms,” *J. Phys. Chem. Lett.* **2022**, 1777–1784 (2022).
- ⁶I. Kozyryev and N. R. Hutzler, “Precision measurement of time-reversal symmetry violation with laser-cooled polyatomic molecules,” *Physical Review Letters* **119**, 133002 (2017).
- ⁷D. DeMille, “Quantum computation with trapped polar molecules,” *Physical review letters* **88**, 067901 (2002).
- ⁸V. V. Albert, J. P. Covey, and J. Preskill, “Robust encoding of a qubit in a molecule,” *Physical Review X* **10**, 031050 (2020).
- ⁹A. Korobenko, A. A. Milner, and V. Milner, “Direct observation, study, and control of molecular superrotors,” *Phys. Rev. Lett.* **112**, 113004 (2014).
- ¹⁰A. Korobenko and V. Milner, “Adiabatic field-free alignment of asymmetric top molecules with an optical centrifuge,” *Phys. Rev. Lett.* **116**, 183001 (2016).
- ¹¹A. A. Milner, A. Korobenko, and V. Milner, “Field-free long-lived alignment of molecules in extreme rotational states,” *Phys. Rev. A* **93**, 053408 (2016).
- ¹²I. Tutunnikov, L. Xu, R. W. Field, K. A. Nelson, Y. Prior, and I. S. Averbukh, “Enantioselective orientation of chiral molecules induced by terahertz pulses with twisted polarization,” *Physical Review Research* **3**, 013249 (2021).
- ¹³D. Patterson and J. M. Doyle, “Sensitive chiral analysis via microwave three-wave mixing,” *Phys. Rev. Lett.* **111**, 023008 (2013).
- ¹⁴M. Leibscher, E. Pozzoli, C. Pérez, M. Schnell, M. Sigalotti, U. Boscain, and C. P. Koch, “Full quantum control of enantiomer-selective state transfer in chiral molecules despite degeneracy,” *Commun. Phys.* **5**, 110 (2022).
- ¹⁵W. Sun, D. S. Tikhonov, H. Singh, A. L. Steber, C. Pérez, and M. Schnell, “Inducing transient enantiomeric excess in a molecular quantum racemic mixture with microwave fields,” *Nat. Commun.* **14**, 934 (2023).
- ¹⁶E. G. Marklund, T. Ekeberg, M. Moog, J. L. P. Benesch, and C. Carleman, “Controlling protein orientation in vacuum using electric fields,” *The Journal of Physical Chemistry Letters* **8**, 4540 – 4544 (2017).
- ¹⁷A. Sinelnikova, T. Mandl, H. Ageli, O. Grånäs, E. G. Marklund, C. Caleman, and E. De Santis, “Protein orientation in time-dependent electric fields: orientation before destruction,” *Biophys. J.* **120**, 3709–3717 (2021).
- ¹⁸Y. Kurosaki, K. Yokoyama, and Y. Ohtsuki, “Quantum control of isotope-selective molecular orientation,” *AIP Conference Proceedings* **2611**, 20010 (2022).
- ¹⁹C. Saribal, A. Owens, A. Yachmenev, and J. Küpper, “Detecting handedness of spatially oriented molecules by Coulomb explosion imaging,” *J. Chem. Phys.* **154**, 71101 (2021).
- ²⁰H. J. Loesch and A. Remscheid, “Brute force in molecular reaction dynamics: A novel technique for measuring steric effects,” *J. Chem. Phys.* **93**, 4779 (1990).
- ²¹J. M. Rost, J. C. Griffin, B. Friedrich, and D. R. Herschbach, “Pendular states and spectra of oriented linear molecules,” *Phys. Rev. Lett.* **68**, 1299–1302 (1990).
- ²²B. Friedrich and D. R. Herschbach, “Enhanced orientation of polar molecules by combined electrostatic and nonresonant induced dipole forces,” *J. Chem. Phys.* **111**, 6157 (1999).
- ²³I. Nevo, L. Holmegaard, J. H. Nielsen, J. L. Hansen, H. Stapelfeldt, F. Filsinger, G. Meijer, and J. Küpper, “Laser-induced 3d alignment and orientation of quantum state-selected molecules,” *Phys. Chem. Chem. Phys.* **11**, 9912 (2009).
- ²⁴J. S. Kienitz, K. Długołęcki, S. Trippel, and J. Küpper, “Improved spatial separation of neutral molecules,” *J. Chem. Phys.* **147**, 024304 (2017).

- ²⁵J. Bulthuis, J. Miller, and H. J. Loesch, "Brute Force Orientation of Asymmetric Top Molecules," *J. Phys. Chem. A* **101**, 7684–7690 (1997).
- ²⁶D. J. Tannor, R. Kosloff, and S. A. Rice, "Coherent pulse sequence induced control of selectivity of reactions: Exact quantum mechanical calculations," *The Journal of Chemical Physics* **85**, 5805–5820 (1986).
- ²⁷J. Werschnik and E. K. U. Gross, "Quantum optimal control theory," *Journal of Physics B: Atomic, Molecular and Optical Physics* **40**, R175 (2007).
- ²⁸C. P. Koch, "Controlling open quantum systems: tools, achievements, and limitations," *Journal of Physics: Condensed Matter* **28**, 213001 (2016).
- ²⁹R. Kosloff, S. A. Rice, P. Gaspard, S. Tersigni, and D. J. Tannor, "Wavepacket dancing: Achieving chemical selectivity by shaping light pulses," *Chemical Physics* **139**, 201–220 (1989).
- ³⁰Q. Ansel, J. Fischer, D. Sugny, and B. Bellomo, "Optimal control and selectivity of qubits in contact with a structured environment," *Phys. Rev. A* **106**, 043702 (2022).
- ³¹L. H. Delgado-Granados, C. A. Arango, and J. G. López, "Preparation of vibrational quasi-bound states of the transition state complex BrHBr from the bihalide ion BrHBr⁻," *Phys. Chem. Chem. Phys.* **24**, 21250–21260 (2022).
- ³²N. Khaneja, T. Reiss, C. Kehlet, T. Schulte-Herbrüggen, and S. J. Glaser, "Optimal control of coupled spin dynamics: design of NMR pulse sequences by gradient ascent algorithms," *Journal of Magnetic Resonance* **172**, 296–305 (2005).
- ³³V. F. Krotov and I. N. Feldmann, "An iterative method for solving optimal-control problems," *Engineering Cybernetics* **21**, 123–130 (1983).
- ³⁴D. J. Tannor, V. Kazakov, and V. Orlov, "Control of Photochemical Branching: Novel Procedures for Finding Optimal Pulses and Global Upper Bounds," in *Time-Dependent Quantum Molecular Dynamics*, edited by J. Broeckhove and L. Lathouwers (Springer US, Boston, MA, 1992) pp. 347–360.
- ³⁵E. Dmitriev and N. Bukharskii, "Powerful Elliptically Polarized Terahertz Radiation from Oscillating-Laser-Driven Discharge Surface Currents," *Photonics* **10**, 803 (2023).
- ³⁶L. H. Coudert, "Optimal orientation of an asymmetric top molecule with terahertz pulses," *The Journal of Chemical Physics* **146**, 024303 (2017).
- ³⁷A. Beer, R. Damari, Y. Chen, and S. Fleischer, "Molecular Orientation-Induced Second-Harmonic Generation: Deciphering Different Contributions Apart," *Journal of Physical Chemistry A* **126**, 3732–3738 (2022).
- ³⁸R. Damari, A. Beer, D. Rosenberg, and S. Fleischer, "Molecular Orientation Echoes via Concerted Terahertz and Near-IR excitations," *Optics Express* **30**, 44464–44471 (2022).
- ³⁹L. H. Coudert, "Optimal control of the orientation and alignment of an asymmetric-top molecule with terahertz and laser pulses," *J. Chem. Phys.* **148**, 094306 (2018).
- ⁴⁰A. Pelzer, S. Ramakrishna, and T. Seideman, "Optimal control of rotational motions in dissipative media," *The Journal of Chemical Physics* **129**, 134301 (2008).
- ⁴¹J. Salomon, C. M. Dion, and G. Turinici, "Optimal molecular alignment and orientation through rotational ladder climbing," *J. Chem. Phys.* **123**, 144310 (2005).
- ⁴²J. J. Omiste, M. Gärttner, P. Schmelcher, R. González-Férez, L. Holmegaard, J. H. Nielsen, H. Stapelfeldt, and J. Küpper, "Theoretical description of adiabatic laser alignment and mixed-field orientation: the need for a non-adiabatic model." *Phys. Chem. Chem. Phys.* **13**, 18815–24 (2011).
- ⁴³W. Kong and J. Bulthuis, "Orientation of asymmetric top molecules in a uniform electric field: Calculations for species without symmetry axes," *J. Phys. Chem. A* **104**, 1055–1063 (2000).
- ⁴⁴R. N. Zare, *Angular Momentum: Understanding Spatial Aspects in Chemistry and Physics* (John Wiley and Sons, New York, 1988).
- ⁴⁵Note that we omit any spatial dependency in the functions for the sake of clarity.
- ⁴⁶Y. Ohtsuki, G. Turinici, and H. Rabitz, "Generalized monotonically convergent algorithms for solving quantum optimal control problems," *Journal of Chemical Physics* **120**, 5509–5517 (2004).
- ⁴⁷T. J. Park and J. C. Light, "Unitary quantum time evolution by iterative Lanczos reduction," *The Journal of Chemical Physics* **85**, 5870–5876 (1986).
- ⁴⁸J. L. Hansen, J. J. Omiste, J. H. Nielsen, D. Pentlehner, J. Küpper, R. González-Férez, and H. Stapelfeldt, "Mixed-field orientation of molecules without rotational symmetry." *J. Chem. Phys.* **139**, 234313 (2013).
- ⁴⁹J. J. Omiste, R. González-Férez, and P. Schmelcher, "Rotational spectrum of asymmetric top molecules in combined static and laser fields." *J. Chem. Phys.* **135**, 064310 (2011).
- ⁵⁰L. V. Thesing, J. Küpper, and R. González-Férez, "Time-dependent analysis of the mixed-field orientation of molecules without rotational symmetry," *Journal of Chemical Physics* **146**, 244304 (2017).
- ⁵¹M. H. Goerz, D. Basilewitsch, F. Gago-Encinas, M. G. Krauss, K. P. Horn, D. M. Reich, and C. P. Koch, "Krotov: A Python implementation of Krotov's method for quantum optimal control," *SciPost Phys.* **7**, 80 (2019).
- ⁵²M. Leibscher, E. Pozzoli, A. Blech, M. Sigalotti, U. Boscain, and C. P. Koch, "Quantum control of ro-vibrational dynamics and application to light-induced molecular chirality," (2023), arXiv:2310.11570.
- ⁵³T. Eriksson, S. Björkman, B. Roth, Å. Fyge, and P. Höglund, "Stereospecific determination, chiral inversion in vitro and pharmacokinetics in humans of the enantiomers of thalidomide," *Chirality* **7**, 44–52 (1995).